Biomaterials 34 (2013) 9171–9182

Contents lists available at ScienceDirect

Biomaterials

journal homepage: www.elsevier.com/locate/biomaterials

LDLR-mediated peptide-22-conjugated nanoparticles for dual-targeting therapy of brain glioma

Bo Zhang [b], Xiyang Sun [a], Heng Mei [b], Yu Wang [a], Ziwei Liao [a], Jun Chen [a], Qizhi Zhang [a], Yu Hu [b,**], Zhiqing Pang [a,*], Xinguo Jiang [a]

[a] School of Pharmacy, Fudan University, Key Laboratory of Smart Drug Delivery, Ministry of Education, 826 Zhangheng Road, Shanghai 201203, PR China
[b] Institute of Hematology, Union Hospital, Tongji Medical College, Huazhong University of Science & Technology, Wuhan, Hubei 430022, PR China

ARTICLE INFO

Article history:
Received 8 July 2013
Accepted 14 August 2013
Available online 3 September 2013

Keywords:
Dual targeting
Low-density lipoprotein receptor
Peptide-22
Nanoparticles
Targeting therapy
Brain glioma

ABSTRACT

Chemotherapy for brain glioma has been of limited benefit due to the inability of drugs to penetrate the blood–brain barrier (BBB) and non-selective drug accumulation in the entire brain. To obviate these limitations, dual-targeting paclitaxel-loaded nanoparticles were developed by decoration with peptide-22 (PNP–PTX), a peptide with special affinity for low-density lipoprotein receptor (LDLR), to transport the drug across the BBB, and then target brain tumour cells. Enzyme-linked immune sorbent assay (ELISA) revealed that LDLR was over-expressed in C6 cells and brain capillary endothelial cells (BCECs), but low LDLR expression was observed in H92c(2-1) cells. Nanoparticle uptake demonstrated that peptide-22-decorated nanoparticles significantly increased the cellular uptake of nanoparticles by C6 cells and BCECs but not by H92c(2-1) cells, and excess free peptide-22 significantly inhibited the cellular uptake of PNP by C6 cells and BCECs. Cellular uptake mechanism experiments showed that PNP uptake by both BCECs and C6 cells was energy-dependant and caveolae- and clathrin-mediated endocytosis pathway other than macropinocytosis were involved. Dual-targeting effects in an in vitro BBB model showed that peptide-22 decoration on nanoparticles loaded with paclitaxel significantly increased the transport ratio of PTX across the BBB and induced apoptosis of C6 glioma cells below the BBB, and these effects were significantly inhibited by excess free peptide-22. Ex vivo and in vivo fluorescence imaging indicated that PNP labelled with a near-infrared dye could permeate the BBB and accumulate more in the glioma site than unmodified NP. Glioma section observed by fluorescence microscopy further demonstrated PNP distributed more extensively in both glioma bulk and infiltrative region around than unmodified NP. Pharmacodynamics results revealed that the median survival time of glioma-bearing mice administered with dual-targeting PNP–PTX was significantly prolonged compared with that of any other group. TUNEL assay and H&E staining showed that PNP–PTX treatment induced significantly more cell apoptosis and tumour necrosis compared with other treatments. Taken together, these promising results suggested that the dual-targeting drug delivery system might have great potential for glioma therapy in clinical applications.

© 2013 Elsevier Ltd. All rights reserved.

1. Introduction

Glioblastoma multiforme (GBM), the most frequent primary central nervous system tumour, has an extremely poor prognosis due to its highly infiltrating nature [1,2]. Those invasive glioma cells are far from the primary tumour or are even in the contralateral hemisphere and hide in areas of the brain that are protected by an intact blood–brain barrier (BBB) [3,4]. Conventional surgical methods cannot completely remove the tumour cell [5,6], and an inevitable relapse always follows. Consequently, a crucial challenge is to deliver therapeutic agents effectively to the tumour core and migratory cells in the infiltration zone [4]. However, existing chemotherapy drugs fail to elicit the desired benefit and are associated with serious adverse effects, largely due to their inability to cross the BBB and untargeted accumulation in healthy tissues [7]. The key point in chemotherapy is to maintain a high concentration of therapeutic agents at the tumour site and prevent their spread

* Corresponding author. Tel./fax: +86 21 51980069.
** Corresponding author. Tel.: +86 27 85726335; fax: +86 27 85776343.
E-mail addresses: dr_huyu@126.com (Y. Hu), zqpang@fudan.edu.cn (Z. Pang).

0142-9612/$ – see front matter © 2013 Elsevier Ltd. All rights reserved.
http://dx.doi.org/10.1016/j.biomaterials.2013.08.039

into the surrounding normal tissues [8]. With this in mind, polymer nanoparticles functioning as a versatile targeting platform are emerging as a good option to address specific existing limitations of conventional chemotherapy [9–11]. Furthermore, dual-targeting nanoparticles targeting both the BBB and glioma tissues functioned better than those targeting each region alone because they could specially deposit in the glioma region whether or not the BBB is compromised [12], and varying degrees of success have been obtained based on the dual-targeting system for glioma therapy [10,13–15].

Low-density lipoprotein receptor (LDLR), a member of the LDLR family, is highly expressed at the BBB [16–18] and has been exploited to transport protein therapeutics across the BBB to reach the CNS [19,20]. Furthermore, LDLR is also over-expressed in a variety of tumour cells, including glioma cells [21–23] but is sub-expressed in normal brain tissues [24,25], making LDLR a potential targeted receptor for brain tumour drug delivery systems, with dual-targeting capability for both the BBB and glioma cells. Although many studies have exploited LDLR as a target for tumour diagnosis [26–28] and treatment [21,29–31], few have extensively explored LDLR as a potential receptor for dual-targeting therapy of brain glioma.

Some targeting moieties such as Apo-B [23], Apo-E [21] and peptides derived from the LDLR binding site of Apo-B [20] or Apo-E [19,32] have been used and have been proven to be effective in LDLR targeted therapy of neurodegenerative disease in CNS or neoplastic diseases. However, they are less than ideal as targeting moieties because of some inherent disadvantages such as protein instability, competition with endogenous LDL as well as the potential risk of disturbing cholesterol homoeostasis in the brain. Recently, phage display biopanning performed by Jean-Daniel Malcor generated a series of peptides, from which peptide-22 (Ac–[cMPRLRGC]c–NH_2) was optimised to show special affinity for LDLR without competition with endogenous LDL and could be efficiently and quickly transferred to the CNS [30]. Therefore, we proposed that the peptide-22–LDLR interaction could be utilised to promote drug delivery across the BBB and simultaneously target brain tumours. Compared with those LDLR-targeting moieties mentioned above, peptide-22 harbours several advantages such as a low molecular weight, good stability, easy synthesis at a relative low cost, lack of immunogenicity [29,31] and even with no competition with endogenous LDL, and may function better in targeting drug delivery [30]. Thus, in the present work, peptide-22 was utilised as a dual-targeting moiety to modify nanoparticles for brain glioma drug delivery.

Paclitaxel (PTX), a major anticancer drug isolated from the bark of *Taxus brevifolia*, showed antitumour activity against various solid tumours such as ovarian cancer, lung cancer [33,34] and glioma [13,35]. However, the therapeutic index of PTX is extremely limited due to its poor aqueous solubility, non-targeted tumouricidal effects and serious side effects associated with its solvent Cremophor EL–ethanol [36]. The therapeutic benefit of PTX against brain tumours could also be compromised by tumour drug-resistance and the inability to readily penetrate the BBB to reach the tumour cells [37,38]. Therefore, a new glioma drug delivery system encapsulating PTX is urgently needed to improve its efficacy and decrease its adverse toxicity.

The objective of the present study was to prepare a dual-targeting drug delivery system, peptide-22-decorated nanoparticles (PNPs). Strongly liposoluble fluorescent probes, courmarin-6 and DiR are used to label PNPs to trace the behaviour of PNPs for their inertia to be released from the polymer nanoparticles [10,39–41]. Dual-targeting delivery properties of PTX-loaded or fluorescence-labelled PNP were evaluated in vitro and in vivo. The in vivo anti-glioma efficacy of PNP–PTX was also investigated using an intracranial glioma mice model.

2. Materials and methods

2.1. Materials and animals

Peptide-22 (NH_2–C6–[cMPRLRGC]c–NH_2) was synthesised by the Chinese Peptide Company (China). Methoxy-poly(ethylene glycol) (MPEG, M_w 3000 Da) was supplied by NOF Corporation (Japan) and R-carboxyl-poly(ethylene glycol) (COOH-PEG, M_w 3400 Da) was obtained from Laysan Bio (AL, USA). D,L-Lactide (purity: 99.5%) was purchased from PURAC (Holland). Methoxy-poly(ethylene glycol)–poly(lactic acid) (MPEG–PLA, M_w 33,000 Da) and R-carboxyl-poly(ethylene glycol)–poly(lactic acid) (COOH-PEG–PLA, M_w 33,400 Da) block copolymers were synthesised by ring-opening polymerisation of lactide using MPEG and HOOC-PEG as the initiator as described elsewhere [42]. Sodium cholate was from Shanghai Chemical Reagent Company. Rat LDLR Elisa Kit was purchased from Shanghai Jianglai Biotechnology Co., Ltd. Courmarin-6, 1-(3-dimethylaminopropyl)-3-ethylcarbodiimide hydrochloride (EDC·HCl) and N-hydroxy-succinimide (NHS) were purchased from Sigma (USA). 1,10-Dioctadecyl-3,3,30,30-tetramethylindotricarbocyanine iodide (DiR), a near-infrared dye, was obtained from Biotium (Invitrogen, USA). The annexin V-FITC apoptosis detection kit, micro-BCA protein assay kit, 4,6-diamidino-2-phenylindole dihydrochloride (DAPI), radio-immunoprecipitation assay (RIPA) and Hoechst 33342 were purchased from Beyotime® Biotechnology Co., Ltd. (Nantong, China). Cellulose ester membranes (dialysis bags) with a molecular weight cut-off value (MWCO) of 8000 Da (Green Bird Inc., Shanghai, China) were used in dialysis experiments. Plastic cell culture dishes and plates were purchased from Corning Incorporation (USA). Dulbecco's modified Eagle's medium (high glucose) (DMEM), foetal bovine serum (FBS), trypsin–EDTA (0.25%) and penicillin–streptomycin were purchased from Gibco (CA). Purified deionised water (Millipore, Bedford, MA) was used throughout the entire study. All other reagents and chemicals were of analytical grade and were purchased from Sinopharm Chemical Reagent (Shanghai, China). Brain capillary endothelial cells (BCECs), C6 cell lines and H9c2(2-1) cells were obtained from the Chinese Academy of Sciences Cell Bank (Shanghai, China). The cells were routinely cultured in Dulbecco's modified Eagle's medium (DMEM, Gibco) supplemented with 10% FBS, 100 IU/ml penicillin and 100 μg/ml streptomycin.

Male BALB/c nude mice and BALB/c mice (20 ± 2 g) were purchased from the Shanghai SLAC Lab Animal Ltd. (Shanghai, China) and maintained under standard housing conditions. All animal experiments were performed in accordance with protocols evaluated and approved by the ethics committee of Fudan University.

2.2. Preparation of unmodified nanoparticles and PNP

Unmodified PEG–PLA nanoparticles (NPs) were prepared using an emulsion/solvent evaporation technique [11] with few modifications. In brief, MPEG–PLA (28 mg) and COOH-PEG–PLA (2 mg) were dissolved in 1 ml of dichloromethane, and then were added into 5 ml of 0.6% sodium cholate aqueous solution. The mixture was intensively emulsified by sonication (200 w, 5 s) fifteen times in ice water using a probe sonicator (Scientz Biotechnology Co., Ltd., China). After evaporating dichloromethane with a ZX-98 rotary evaporator (Shanghai Institute of Organic Chemistry, China) at 37 °C, the obtained nanoparticles were concentrated by centrifugation at 14,500 rpm for 45 min using a TJ-25 centrifuge (Beckman Counter, USA). After discarding the supernatant, the nanoparticles were resuspended in 0.5 ml of deionised water. PTX-loaded, coumarin-6- or DiR-labelled NPs were prepared using the same procedure except that 2 mg PTX, 30 μg of coumarin-6 or 200 μg of DiR were dissolved in 1 ml of dichloromethane in advance.

Peptide-22 was conjugated to the surface of NPs using an EDC/NHS technique [9]. In brief, NP was suspended in deionised water and incubated with excess EDC (200 mM) and NHS (100 mM) at room temperature for 30 min. The resulting N-hydroxysuccinimide-activated NP was then centrifuged at 14,500 rpm for 45 min to remove the residual EDC and NHS. The activated NP was allowed to react with 20 μg of peptide-22 under magnetic stirring for 4 h. Thereafter, the covalently linked PNP was concentrated by centrifugation at 14,500 rpm for 45 min to remove free peptide-22. PTX-loaded, coumarin-6- and DiR-labelled PNP were prepared using the same procedure.

2.3. Characterisation of PNP

Particle size and zeta potential of nanoparticles were determined by dynamic light scattering using a zeta plus analyser (Zeta-sizer, Malvern nano zs, U.K.). The morphology of nanoparticles was observed using a transmission electron microscope (H-600; Hitachi, Japan) after negative staining with 2% sodium phosphotungstate solution.

2.4. Determination of peptide-22 conjugation efficiency and peptide-22 density on the nanoparticle surface

The concentration of peptide-22 in the supernatant was determined using an HPLC system (Agilent 1200 series; USA) with an analytical column (150 mm × 4.6 mm; pore size 5 μm; ZORBAX 300SB-C_{18}; Agilent). The mobile phase contained a mixture of solvent A (0.1% trifluoroacetic acid in water) and solvent B

(80% acetonitrile solution containing 0.09% trifluoroacetic acid) (A:B = 75:25, *v*/*v*) at a flow rate of 1.0 ml/min. The sample injection volume was 20 μl, and the detector wavelength was 220 nm. The peptide-22 conjugation efficiency was calculated as follows: Conjugation efficiency = (total amount − the amount in supernatant)/total amount × 100%. The peptide-22 density on the nanoparticle surface was calculated as previously described [39,43].

2.5. Drug encapsulation efficiency and loading capacity

The drug encapsulation efficiency (EE) and loading capacity (LC) of PTX-loaded NP (NP–PTX) and PTX-loaded PNP (PNP–PTX) were investigated as previously described [29]. Briefly, NP–PTX or PNP–PTX was dissolved in acetonitrile, vortexed for 1 min and subjected to centrifugation at 10,000 rpm for 10 min using a 5418-R centrifuge (Eppendorf, Germany) to thoroughly remove the polymer materials. The PTX concentration in the supernatant was determined by the HPLC system (Agilent 1200, USA) equipped with an analytical column (150 mm × 4.6 mm, pore size 5 μm, Diamonsil™, Dikma). The mobile phase was a mixture of acetonitrile and water (CH_3CN:H_2O = 55:45, *v*/*v*) at a flow rate of 1.0 ml/min. The sample injection volume was 20 μl, and the detector wavelength was 227 nm. The encapsulation efficiency was calculated as EE = $PTX_{encapsulated}/PTX_{total}$ × 100% and drug loading capacity was calculated as LC = $PTX_{encapsulated}$/materials × 100%.

2.6. In vitro release profiles

The in vitro release behaviours of PTX from NP–PTX and PNP–PTX were evaluated by a dialysis method using PBS (0.01 M, pH 7.4) with 0.5% Tween-80 as the release medium [44]. For the experiment, 1 ml of the PTX formulation (containing 60 μg of PTX) was introduced into a dialysis bag (MWCO 8000 Da; Green Bird Inc., Shanghai, China) and incubated in 10 ml of release medium at 37 °C at the shaking speed of 120 rpm for 48 h. At each setting time point, 0.3 ml of aliquot was withdrawn and, immediately, an equal volume of fresh release medium was added. The amount of PTX was determined by the same method mentioned above.

2.7. LDLR expression level in targeted cells

C6 cells were seeded at a density of 5×10^5 cells per dish in 5.5-cm^2 dishes, and then were incubated for 48 h. When the cell confluency reached 80%, the cells were washed three times with cold PBS, harvested with a scraper, centrifuged at 3000 rpm for 3 min, and then subjected to lysis in 100 μl of RIPA buffer. The total protein content and LDLR content in the cell lysates were measured using a micro BCA kit and LDLR Elisa kit, respectively. The LDLR expression level was defined by the proportion of LDLR content in the total protein content. The LDLR expression level in BCECs and H9c2(2-1) cells was determined using the same method as described above.

2.8. In vitro cellular uptake of coumarin-6-labelled PNP

For cellular uptake examination, H9c2(2-1) cells, BCECs and C6 cells were seeded at a density of 2×10^4 cells per well in 24-well plates, incubated for 24 h, and checked under the microscope for cell confluency and morphology. When the cells reached about 80% confluency, the medium was replaced with 500 μl of culture medium containing coumarin-6-labelled NP or PNP, and the cells were incubated for 45 min at 37 °C. The concentration of coumarin-6 in each well was adjusted to 20 ng/ml. For qualitative analysis, the cells were washed three times with cold PBS, mounted in Dako fluorescent mounting medium, and then observed under a fluorescent microscope (Leica, Germany). For quantitative analysis, the cells were harvested, suspended in 0.5 ml PBS and subjected to flow cytometry using a FACS Aria Cell Sorter (BD, USA) as described previously [11]. To further confirm the potential of peptide-22 in mediating the uptake of PNP, BCECs and C6 cells were incubated with excess peptide-22 (200 μg/ml) for 30 min in advance, followed by the same steps mentioned above.

2.9. Cellular uptake mechanism of PNP

C6 cells and BCECs were seeded in 12-well plates at the density of 1×10^5 cells/well and cultured for 24 h. After a 30-min incubation in DMEM, the cells were treated with coumarin-6-labelled PNP (20 ng/ml of coumarin-6) and with various endocytic inhibitors including DMEM (control), NaN_3 (0.1%), filipin (10 μg/ml), chlorpromazine hydrochloride (CPZ, 20 μg/ml), cytochalasin B (Cyto-B, 40 μM), monensin (100 nM) and brefeldin A (BFA, 20 μg/ml). After 60-min incubation, the nanoparticles suspension was removed, and the cells were washed three times with ice-cold PBS, subsequently with acid buffer (consisting of 120 mM NaCl, 20 mM sodium barbital, and 20 mM sodium acetate, pH 3) at 4 °C for 5 min, and again with ice-cold PBS [45]. Afterward, the cells were harvested by trypsinization and analysed by flow cytometry using a FACS Aria Cell Sorter (BD, USA). PNP uptake was presented as the relative fluorescence intensity (%) of the control.

2.10. Transport across the BCEC monolayer of PNP

BCECs were seeded at a density of 5×10^4 cells/well onto polycarbonate 24-well Transwell membranes with a 1.0-μm mean pore size and 0.33-cm^2 surface area (FALCON Cell Culture Insert, Becton Dickinson Labware, USA). Before starting the experiment, the tightness of the cell monolayer was monitored by measuring the trans-endothelial electrical resistance (TEER) using an epithelial volt ohmmeter (Millicel-RES, Millipore, USA). Only cell monolayers with TEER above 200 Ω cm^2 were used for further experiments [46]. To evaluate the ability of the carriers across the BBB, the transport ratio (%) was measured using 10% FBS-containing DMEM as the transport medium. Different PTX formulations, including Taxol, NP–PTX and PNP–PTX, were added into the donor chamber at a PTX concentration of 10 μg/ml and incubated at 37 °C. A volume of 300 μl of the sample was taken from the acceptor compartment at 2 h, 4 h, 8 h, 12 h and 24 h, and 300 μl of fresh medium was supplemented immediately after each sampling. For PTX concentration determination, the samples were added in 3-fold volumes of acetonitrile to precipitate protein and extract PTX. The mixture was vortexed for 1 min, and subsequently centrifuged at 12,000 rpm for 10 min. The supernatant was subjected to liquid chromatography-tandem mass spectrometry (LC-MS/MS) analysis (Agilent 1100 series LC/MSD, America). Ion detection was conducted in the single ions monitoring (SIM) mode, monitoring the *m*/*z* 876.2 for paclitaxel ($M + Na^+$). For the competition assay, an excess of peptide-22 (200 μg/ml) was added to the donor chamber and incubated at 37 °C for 30 min in advance. The compounds were then replaced with the PNP–PTX suspension at a PTX concentration of 10 μg/ml followed by the above mentioned steps. TEER was measured to monitor the integrity of the BCEC monolayer during the experiment.

2.11. Dual-targeting effects of PNP–PTX in vitro

The BCECs-C6 cells co-culture model was established to analyse the potential dual-targeting effects of PNP in vitro [10,13]. In brief, the BCECs monolayer model was established as described above. After the TEERs of the BCECs monolayer reached above 200 Ω cm^2, the transwells were transferred to another 24-well culture plate with confluent C6 cells. After co-culture for 24 h, the co-cultured model was incubated with different PTX formulations including Taxol, NP–PTX, and PNP–PTX at a PTX concentration of 10 μg/ml in donor chambers. For the competition assay, the co-cultured model was incubated with excess peptide-22 (200 μg/ml) for 30 min before incubation with PNP–PTX. After 8-h incubation, the inserts were removed, and C6 cells were further cultured for another 24 h. Cell apoptosis activity was then evaluated. For qualitative assays, cells were fixed with 4% paraformaldehyde followed by Hoechst 33342 staining (2 μg/ml), and then were observed using a fluorescent microscope (Leica, Germany). For quantitative assays, cells were stained using the Annexin V-FITC Apoptosis Detection kit and analysed by a FACS Aria Cell Sorter (BD, USA).

2.12. Ex vivo imaging of PNP in normal mice

BALB/c mice were randomly divided into two groups: the NP and PNP groups. Each mouse was injected with DiR-labelled NP or PNP (containing 10 μg of DiR) via the tail vein. At 1 h, 2 h, 4 h, 7 h and 10 h post-injection, the mice from each group were sacrificed to harvest the brains. Ex vivo fluorescence imaging and the fluorescence intensity of these brains were obtained using a Maestro in vivo imaging system (Cri, USA) [47].

2.13. In vivo imaging of PNP in glioma-bearing mice

The C6 orthotopic glioma model was established by injection of C6 cells (5×10^5 cells in 5 μl of PBS (0.01 M, pH 7.4)) into the right brain of each nude mouse (2 mm lateral to the bregma and 5.0 mm deep from the dura) at a rate of 3.0 μl/min using a stereotaxic apparatus. Ten days after implantation, DiR-labelled PNP and NP were injected into the tail vein of mice at a dose of 10 μg of DiR. The in vivo imaging was performed at different time points (2 h, 6 h, 12 h and 24 h) post-injection using the In Vivo IVIS spectrum imaging system (PerkinElmer, USA). At 24 h post-injection, the mice were sacrificed and the brains and other major organs were harvested and the ex vivo imaging of the organs was also captured.

2.14. In vivo glioma distribution of PNP

The glioma-bearing mice were established as described above. Eight hours after administration with DiR-labelled PNP and NP, the mice were anesthetised with i.p. administered 5% chloral hydrate followed by heart perfusion with saline and 4% paraformaldehyde. Subsequently, the brains were removed, fixed in 4% paraformaldehyde for 24 h, and dehydrated with 15% sucrose solution until subsidence and 30% sucrose solution until subsidence. Thereafter, the brains were frozen in OCT (Sakura, Torrance, CA, USA) at −80 °C and cut into 20-μm sections. After counterstaining with 1 μg/ml DAPI for 10 min at room temperature, slides were observed using a fluorescence microscope (Leica, Germany).

2.15. In vivo anti-glioblastoma effect of PNP–PTX

BALB/c mice bearing intracranial C6 glioma were established as described above. The mice were randomly divided into four groups (16 mice per group) and injected with 100 μl of PNP–PTX, NP–PTX, Taxol (PTX dose of 6 mg/kg) and saline via the tail vein at 5, 8, 11 and 14 days after C6 cells implantation. At days 10 and 13, three mice from each group were sacrificed, and the brains were harvested. The brains were fixed with 10% neutral formalin for 48 h, embedded in paraffin and cut into 5-μm sections, followed by haematoxylin and eosin (H&E) staining using routine protocols and Tdt-mediated dUTP nick-end labelling (TUNEL) using the protocol of the NeuroTACS II in situ apoptosis detection kit. Ten tumour-bearing mice from each group were followed by survival monitoring, and the survival data were analysed using the log-rank test.

3. Results

3.1. Characterisation of the nanoparticles

As shown in Table 1, the particle sizes were 110.8 nm and 129.6 nm for NP and PNP, respectively. Conjugation with peptide-22 slightly increased the particle size and decreased the zeta potential. However, encapsulation of coumarin-6, DiR or PTX did not significantly influence the particle size. TEM photograph showed that the PNP was spherical in shape and had a smooth surface with a uniform distribution (Fig. 1A). The particle size observed by TEM was similar but slightly smaller than that obtained from the DLS method (Fig. 1B). Under our experimental conditions (molar ratio of COOH-PEG–PLA to peptide-22 = 3:1, reaction time = 4 h), the peptide-22 conjugation efficiency was approximately 35.8%, and the peptide-22 density on the nanoparticle surface was approximately 248 molecules per nanoparticle. The LC values of NP–PTX and PNP–PTX were 2.61 ± 0.045% ($n = 3$) and 2.0 ± 0.049% ($n = 3$), respectively. Additionally, the EE values of PTX were 33.1 ± 0.57% ($n = 3$) and 29.1 ± 0.67% ($n = 3$) for NP–PTX and PNP–PTX, respectively. The in vitro release profiles of NP–PTX and PNP–PTX displayed a similar biphasic pattern (Fig. 1C), suggesting that modification of peptide-22 did not evidently influence the in vitro release behaviour of nanoparticles.

3.2. Receptor expression level in targeted cells

The LDLR expression level in H9c2(2-1) cells, BCECs and C6 cells was 1.47, 6.36, and 8.0 ng/mg of protein, respectively (Fig. 2). LDLR is highly expressed in BCECs and C6 cells, but much less in myocardial cells, which might serve as a negative control to evaluate the function of the targeted receptor LDLR.

3.3. Cellular uptake of coumarin 6-labelled PNP

As shown in Fig. 3, fluorescent microscopy and flow cytometry results demonstrated that the fluorescence intensities of C6 cells and BCECs treated with coumarin-6-labelled PNP were significantly higher than those treated with coumarin-6-labelled NP but significantly decreased by pre-incubation of C6 cells and BCECs with excess free peptide-22, suggesting that peptide-22 decoration on nanoparticles surface could significantly facilitate the uptake of nanoparticles by LDLR over-expressed C6 cells and BCECs but this facilitation could be inhibited by excess free peptide-22. However, as to LDLR sub-expressed H9c2(2-1) cells, there was no significant difference in the fluorescence intensity between the NP group and PNP group, indicating peptide-22 decoration did not change the uptake behaviour of nanoparticles by LDLR sub-expressed H9c2(2-1) cells. Considering that peptide-22 could specifically bind to LDLR, these results indicated that LDLR might involve in the cellular uptake of PNP by LDLR over-expressed cells and peptide-22 might facilitate PNP to transport across the BBB and simultaneously target to the glioma cells.

3.4. Cellular uptake mechanism of PNP

In order to elucidate the cellular uptake mechanism of PNP, the effects of ATP depletion and different endocytosis inhibitors on PNP uptake were evaluated in BCECs and C6 cells. As shown in Fig. 4, the uptake of PNP by BCECs was significantly inhibited by NaN_3 (energy depletion agent), filipin (caveolae-mediated endocytosis inhibitor) and CPZ (clathrin-mediated endocytosis inhibitor), but not by Cyto-B (macropinocytosis inhibitor), BFA (disrupting the Golgi apparatus and intracellular trafficking) and monensin (lysosome inhibitor). As to C6 cells, the uptake of PNP was significantly suppressed by NaN_3, filipin, CPZ and BFA, but not by Cyto-B and monensin. These results indicated that PNP uptake by both BCECs and C6 cells was energy-dependant and caveolae- and clathrin-mediated endocytosis pathway but not macropinocytosis were involved.

3.5. In vitro BBB transportation of PNP–PTX

In vitro BBB model was established and TEER value (>200 Ω cm^2) was monitored to validate the reliability of this model. No obvious reduction in the TEER values was seen during the whole experiment, indicating that the transport of drug did not compromise the BBB barrier properties. As shown in Fig. 5, the transport ratios of PTX for all groups increased with time, showing a time-dependent pattern. In addition, the transport ratio of PTX for PNP–PTX group was significantly higher than that for any other group at the same time point. After 24-h incubation, the transport ratio for PNP–PTX reached 24.78% which is 1.60-fold higher than that for NP–PTX group (15.51%), and 2.59-fold higher than that for Taxol group (9.57%), indicating the peptide-22 decoration enhanced the transport capability of drug-loaded nanoparticles across the BBB. Moreover, pre-incubation with excess peptide-22 to saturate the binding site of LDLR at the BBB significantly decreased the transport ratio of PTX for the PNP–PTX group, suggesting that LDLR might mediate the transport of PNP–PTX across the BBB.

3.6. Dual-targeting effects of PNP–PTX in vitro

The dual-targeting effects of PNP–PTX was evaluated by the BCECs-C6 cell co-culture model where different PTX formulations crossed the BCECs monolayer, and then apoptosis was induced in C6 cells under the BCECs monolayer. As shown in Fig. 6, the PNP–PTX group produced the strongest cytotoxicity against C6 cells among all PTX formulations. The nuclei of the control group were spherical and integrated with homogeneous fluorescence after Hoechst 33342 staining. By contrast, PTX formulation treatment led to segregation of the cell nuclei into segments, indicating the nuclei were condensed and further distributed into apoptotic bodies. The result was consistent with that of the quantitative assay by flow

Table 1
Size and zeta potential of nanoparticles ($n = 3$).

	NP	NP–cou-6	NP–DiR	NP–PTX	PNP	PNP–cou-6	PNP–DiR	PNP–PTX
Size (nm)	110.8 ± 1.8	112.9 ± 3.4	123.8 ± 6.5	120.1 ± 1.7	129.6 ± 2.1	128.4 ± 2.6	137.4 ± 4.9	124.7 ± 2.7
Zeta potential (mv)	−10.7 ± 0.2	−10.0 ± 0.4	−9.7 ± 0.5	−10.3 ± 0.7	−29.6 ± 3.6	−28.2 ± 0.6	−30.1 ± 1.6	−29.2 ± 0.8

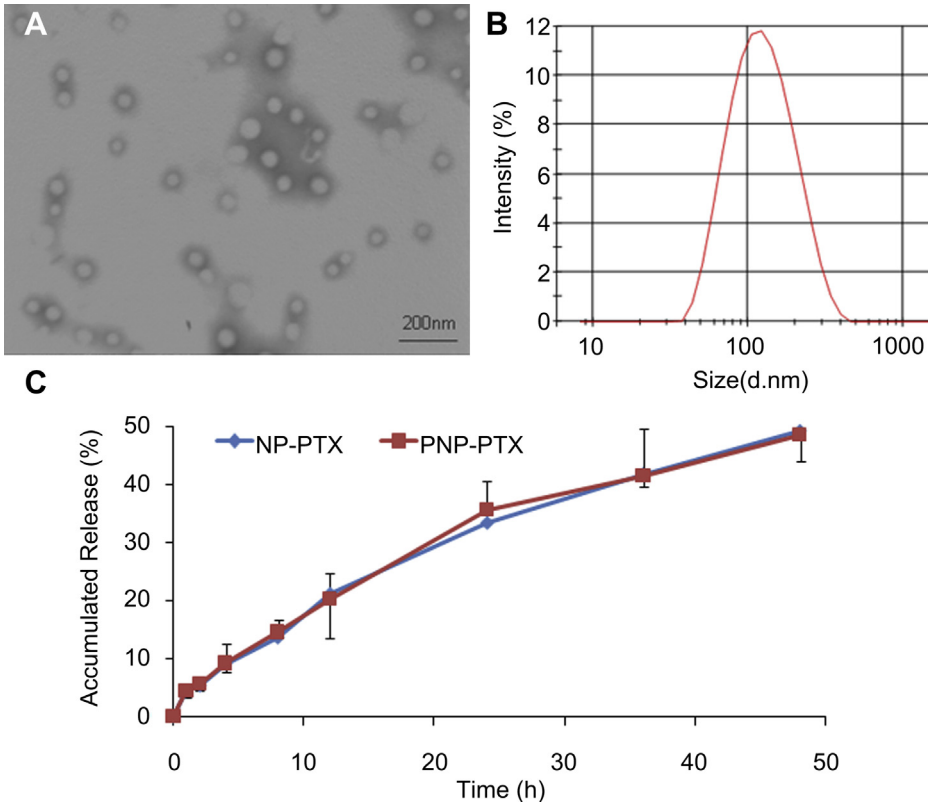

Fig. 1. (A) The transmission electron microscope image of PNP. (B) The particle size distribution of PNP. (C) The releasing profiles of PTX from NP–PTX and PNP–PTX in PBS (0.01 M, pH 7.4) with 0.5% Tween-80 at 37 °C. The bar represents 200 nm.

cytometry. Compared with the Taxol-treated group with early and late apoptosis percentages of 0.98 ± 0.53% and 2.23 ± 0.44%, respectively, the PNP–PTX-treated group caused significantly higher early and late cell apoptosis, 9.25 ± 0.45% ($P < 0.001$) and 6.06 ± 1.41% ($P < 0.05$), respectively. Regarding the NP–PTX group, the early and late apoptosis percentages were 3.92 ± 0.79% and 3.39 ± 0.6%, respectively. Compared with the NP–PTX group, PNP–PTX treatment significantly caused early apoptosis ($P < 0.01$) and enhanced the late apoptosis to some degree without significance. However, pre-incubation with excess free peptide-22 caused the percentage of early apoptosis for PNP–PTX to be significantly inhibited to 4.36 ± 1.76% ($P < 0.05$), and the percentage of late apoptosis was decreased to 3.70 ± 0.54% without significance ($P = 0.087$). Concerning total apoptosis, PNP–PTX treatment induced significantly more apoptosis of C6 cells compared with any other group ($P < 0.05$).

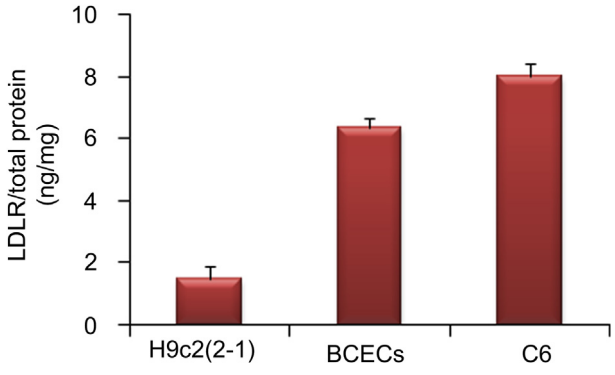

Fig. 2. LDLR expression in H9c2(2-1) cells, BCECs and C6 cells.

3.7. In vivo evaluation of brain targeting of PNP

To investigate the brain-targeting capability of PNP, ex vivo fluorescence images of the brains were acquired after i.v. administration with DiR-labelled PNP and NP. As shown in Fig. 7, the brain fluorescence intensity for the PNP group was significantly higher than that for the NP group at 1 h, 2 h, 4 h, 7 h and 10 h post-injection. In addition, according to the semi-quantitative fluorescence intensity–time curve, the area under the curve (AUC_{0-t}) of PNP was 2.3 times higher than that of NP. The results confirmed that PNP could cross the BBB and penetrate the brain more efficiently than NP, findings that might be attributed to the interaction between peptide-22 and LDLR over-expressed at the BBB.

3.8. In vivo imaging of PNP in glioma-bearing mice

To investigate the glioma-targeting capability of PNP, in vivo imaging of glioma-bearing mice treated with DiR-labelled PNP or NP was performed. As shown in Fig. 8A, the fluorescence intensity in the brain of PNP-treated mice was significantly higher than that in NP-treated mice at any time point post-administration. The ex vivo imaging of the brains at 24 h showed that the fluorescence intensity in normal brain tissues and glioma tissues for the PNP group was 1.37-fold and 2.48-fold as that for NP group (Fig. 8A&C), indicating that PNP accumulated more than NP in glioma related region. Furthermore, the glioma/brain fluorescence ratios were 2.17 and 3.95 for NP and PNP, respectively, demonstrating that PNP with the dual-targeting capacity had a higher selectivity for malignant glioma tissues than NP. As to other major organs, PNP distribution was almost the same as NP (Fig. 8B&D), mainly distributed in the mononuclear phagocyte system (MPS)-related organs including liver and spleen.

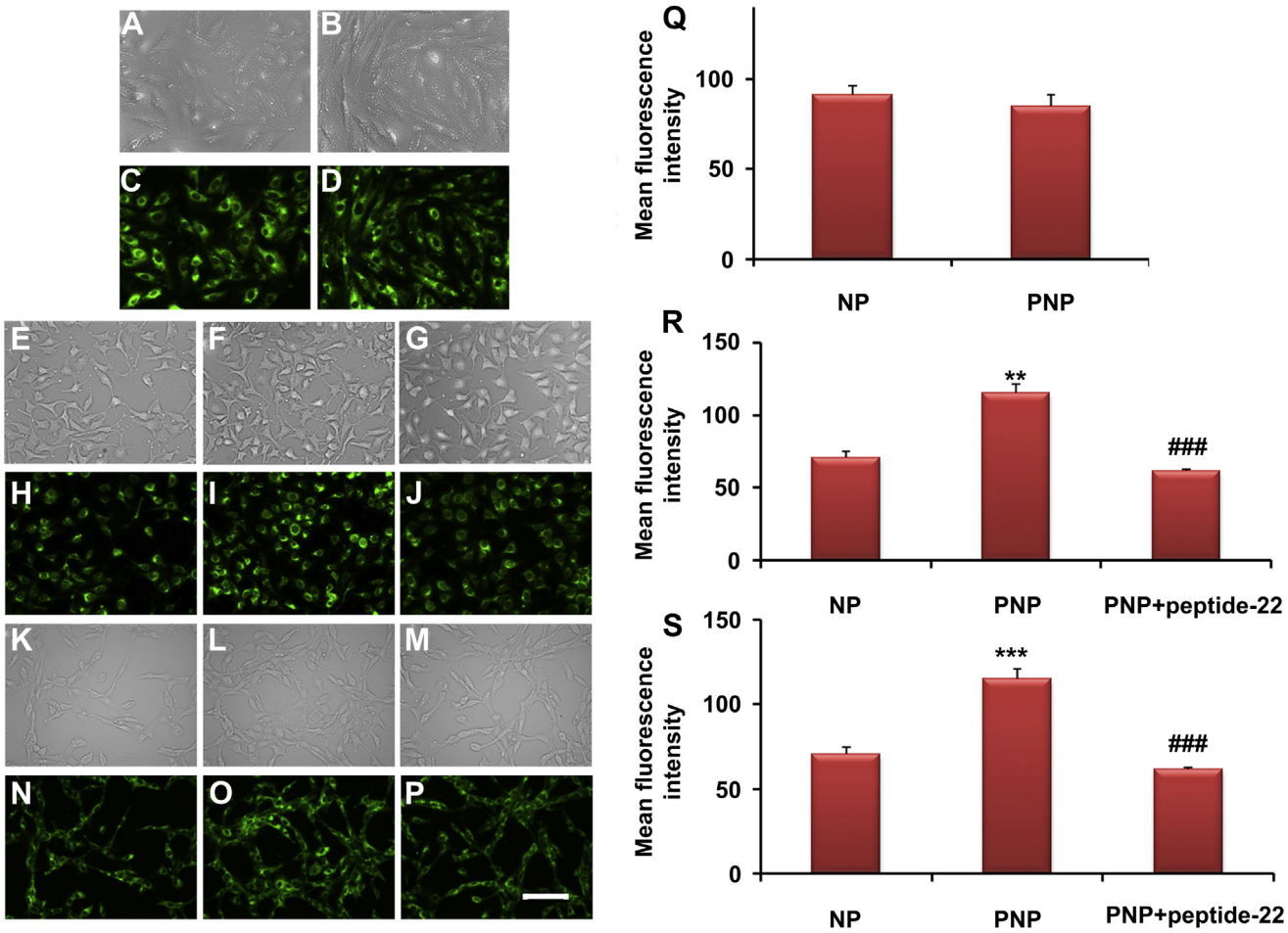

Fig. 3. Qualitative and quantitative measurement of in vitro uptake of coumarin-6-labelled NP (A, C, E, H, K, N), PNP (B, D, F, I, L, O) and PNP plus 200 μg/ml of free peptide-22 (G, J, M, P) by H9c2 (2-1) cells, BCECs and C6 cells after 45 min of incubation. The concentration of coumarin-6 in all samples was adjusted to 20 ng/ml. Bright light images for H9c2 (2-1) cells (A, B), BCECs (E, F, G) and C6 cells (K, L, M). Fluorescent images for H9c2 (2-1) cells (C, D), BCECs (H, I, J) and C6 cells (N, O, P). Flow cytometry results for H9c2 (2-1) cells (Q), BCECs (R) and C6 cells (S). Green: coumarin-6. The bar represents 200 μm. Statistically significant difference by Student's *t*-test when compared to the corresponding value of control. $^{**}P < 0.01$, $^{***}P < 0.001$ vs NP. $\#\#\#P < 0.001$ vs PNP. (For interpretation of the references to colour in this figure legend, the reader is referred to the web version of this article.)

3.9. *In vivo glioma distribution of PNP*

The in vivo glioma targeting of DiR-labelled PNP was studied qualitatively by fluorescence microscopic observation of coronal sections of the orthotopic glioma-bearing mouse brain. It was shown that only a few red particles of DiR-labelled NP were distributed in the glioma region due to enhanced permeation and retention effect (EPR effect) (Fig. 9D–F), but a significantly higher distribution of DiR-labelled PNP at the glioma site was observed

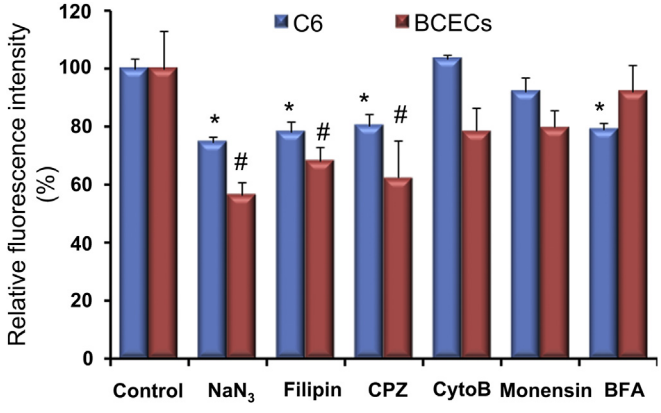

Fig. 4. Cellular uptake of coumarin-6-labelled PNP by BCECs and C6 cells in the presence of NaN_3 (0.1%), filipin (10 μg/ml), chlorpromazine (20 μg/ml), cytoB (40 μM), monensin (100 nM), BFA (20 μg/ml), respectively ($n = 3$). Statistically significant difference by Student's *t*-test when compared to the corresponding value of control. $^{*}P < 0.05$, vs C6 cells control. $\#P < 0.05$ vs BCECs control.

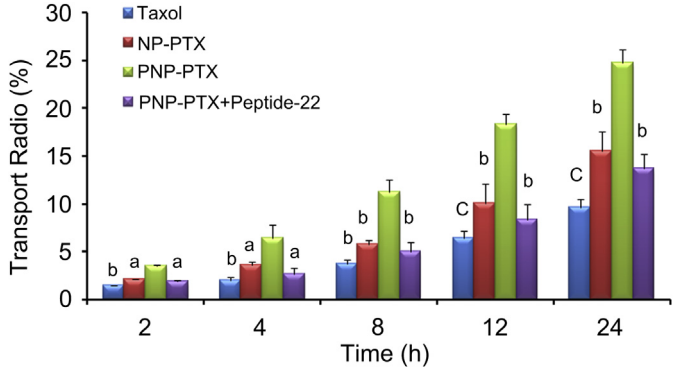

Fig. 5. The transport ratio (%) of PTX across the in vitro BBB model during 24 h. Data were presented as mean ± standard deviation ($n = 3$). Statistically significant differences by Student's *t*-test when compared to the corresponding value of the control. $^{a}P < 0.05$; $^{b}P < 0.01$; $^{c}P < 0.001$, vs PNP–PTX.

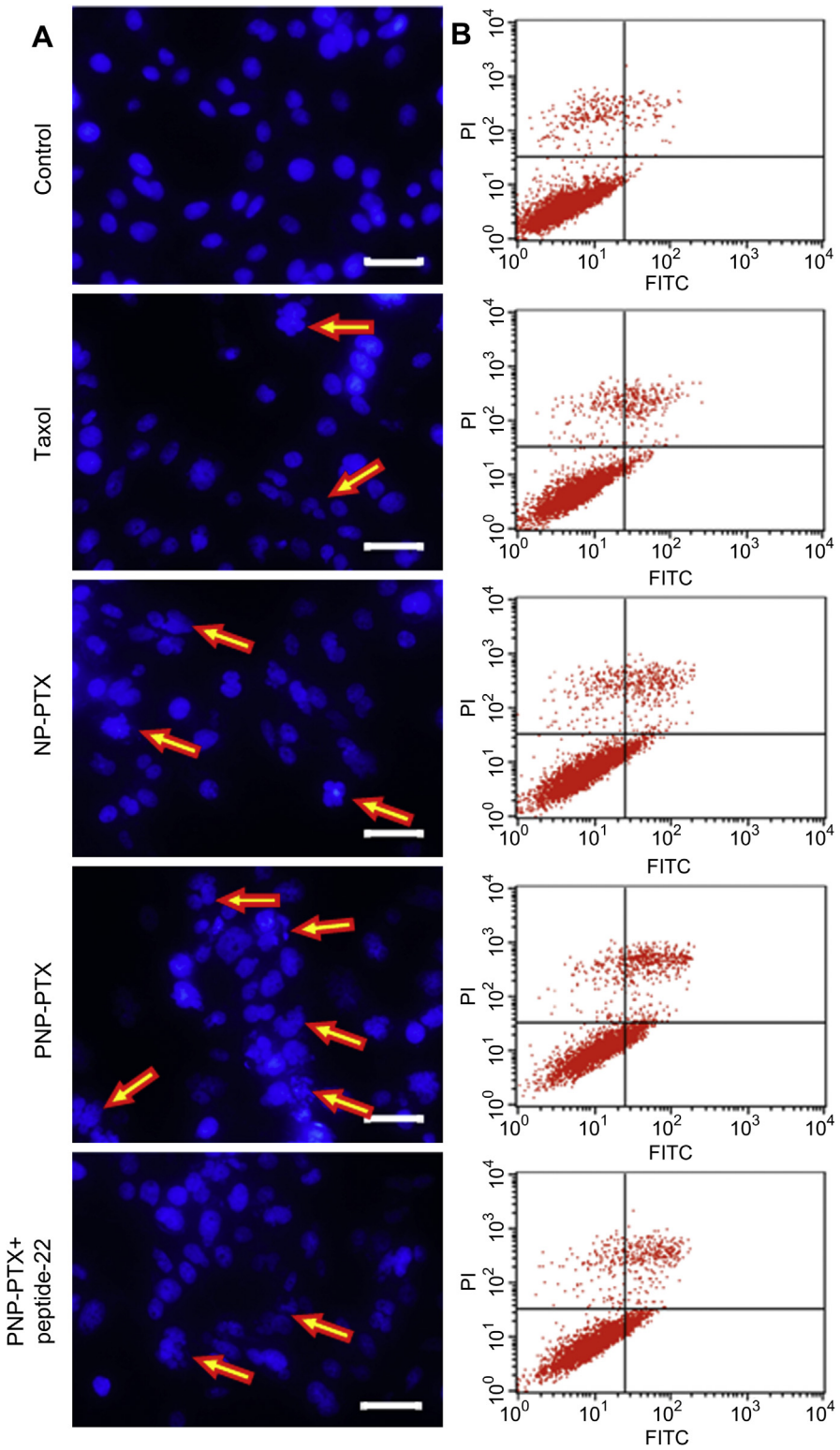

Fig. 6. Dual-targeting effects in vitro. Cell apoptosis induced by Taxol, NP–PTX, PNP–PTX, PNP–PTX and free peptide-22 against C6 cells after crossing the BBB in vitro ($n = 3$). Fluorescence micrographs of C6 cell nuclei stained with Hoechst 33342 (A) and flow cytometry results after staining with Annexin V-FITC and PI (B). Arrows indicate cell apoptosis. The bar represents 100 μm.

(Fig. 9A–C). Because of the equal contribution of the EPR effect to the NP and PNP groups in tumour sites, the enhancement of penetration and distribution in the glioma region of PNP might result from active targeting via LDLR-mediated endocytosis. In cancerous brain tissues surrounding the glioma, PNP also showed better penetration than NP (B and E), a finding that was consistent with those obtained from NP and PNP distribution in normal mice (Fig. 7) and glioma-bearing mice (Fig. 8A).

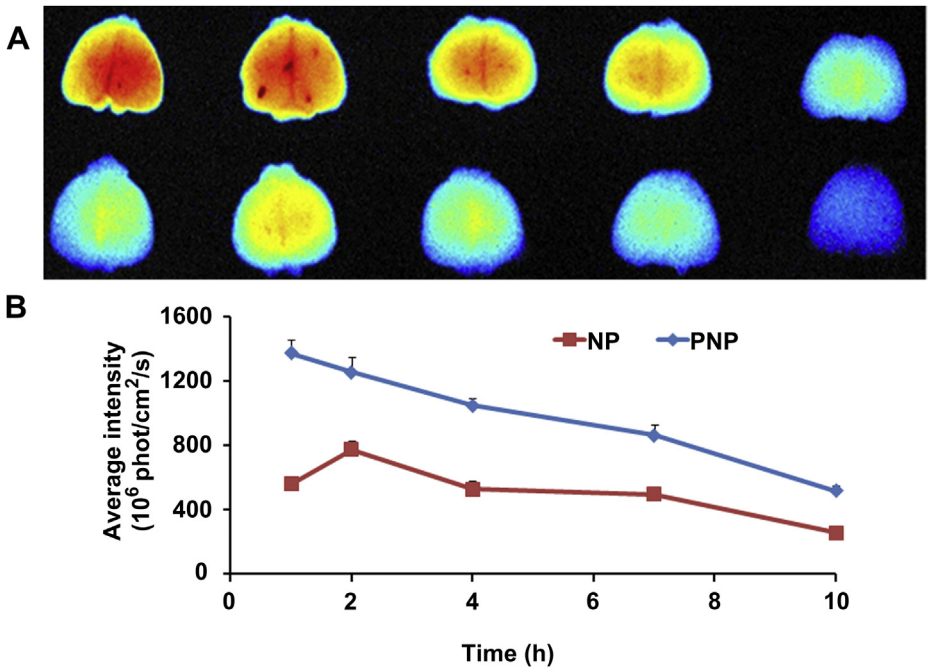

Fig. 7. (A) Ex vivo fluorescence imaging of mouse brains at various time points (from left to right: 1 h, 2 h, 4 h,7 h, 10 h) after i.v. administration of DiR-labelled PNP (upper row) and NP (lower row) and (B) the corresponding semi-quantitative results.

3.10. *In vivo anti-glioblastoma effect of PNP–PTX*

To assess the antitumour effects of PNP–PTX, the survival time of intracranial C6 glioblastoma-bearing mice was studied. Life-span extension treated with a multi-dose of 6 mg/kg PTX on days 5, 8, 11 and 14 after glioma implantation was shown in Fig. 10. Using the log-rank test, the median survival time for control group, Taxol group, NP–PTX group and PNP–PTX group were 14, 13, 21 and 32 days, respectively. Compared with the control group, PNP–PTX ($P < 0.001$) and NP–PTX treatment ($P < 0.05$) significantly prolonged the survival time, in sharp contrast with Taxol® treatment, which resulted in no significant prolongation in the survival time ($P > 0.05$). However, the increase in survival time (IST) of the PNP–PTX group was more considerable when compared with NP–PTX,

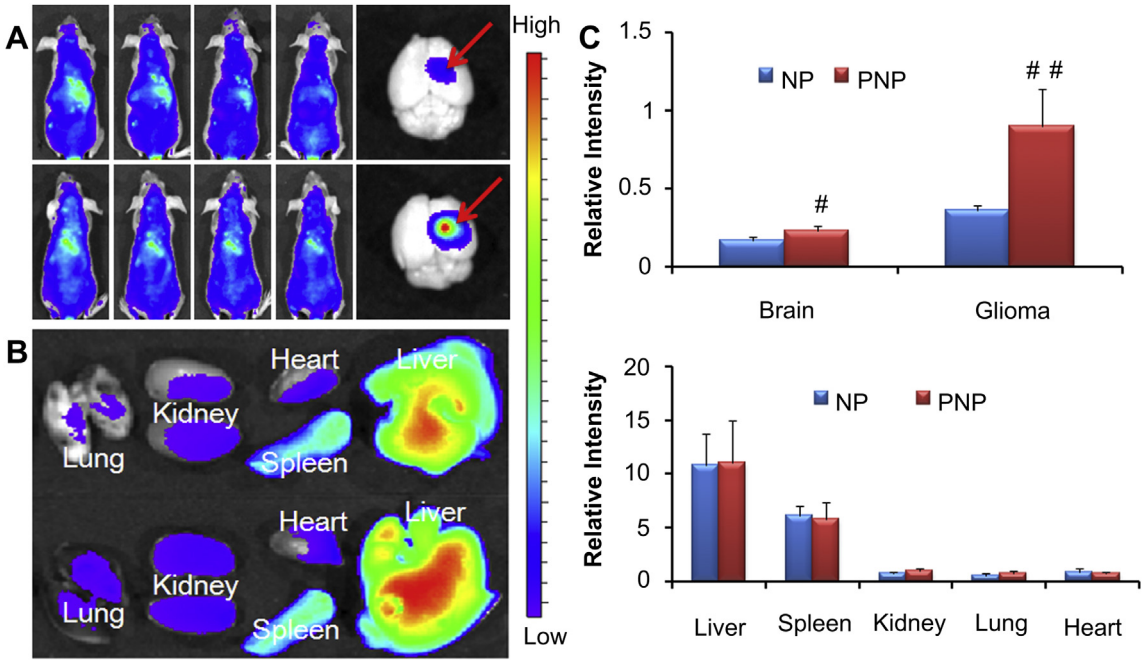

Fig. 8. (A) In vivo imaging of DiR-labelled NP (upper row) and PNP (lower row) at different time points post i.v. injection (from left to right: 2 h, 6 h, 12 h, 24 h) and ex vivo imaging of the brains harvested at 24 h. (B) Ex vivo imaging of other major organs at 24 h. (C) Semi-quantitative fluorescence intensity of brain and glioma. (D) Semi-quantitative fluorescence intensity of different organs. The red arrow indicates glioma. Statistically significant differences by Student's *t*-test when compared to the corresponding value of the control. ##$P < 0.01$, #$P < 0.05$, vs NP. (For interpretation of the references to colour in this figure legend, the reader is referred to the web version of this article.)

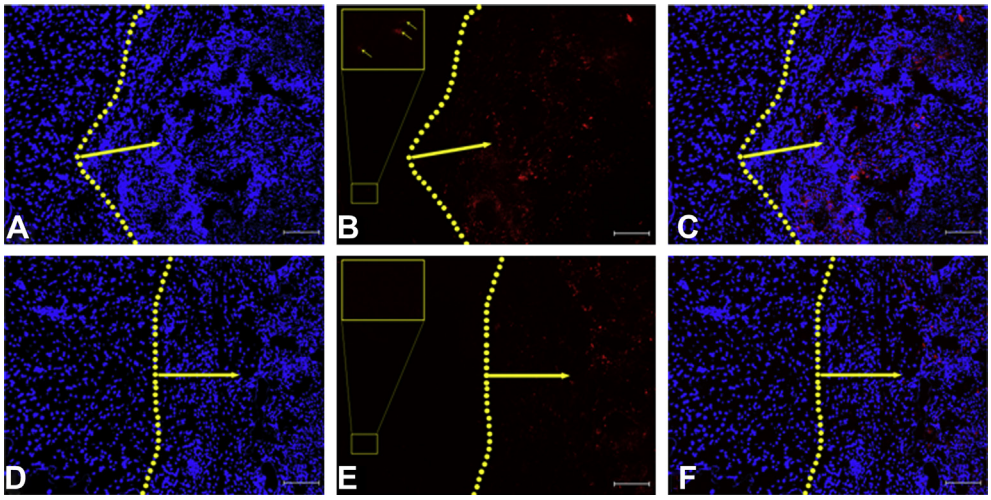

Fig. 9. Distribution of Dir-labelled nanoparticles in the brains of glioma-bearing nude mice treated with DiR-labelled PNP (A–C) and DiR-labelled NP (D–F) 8 h after intravenous administration. Figure C is the merged image of A and B, and F is the merged image of D and E. Red: DiR. Blue: cell nuclei. Yellow line: the border of the glioma. Yellow arrow: the direction of the glioma. The images of the inner boxes of Figures B and E represent PNP and NP distribution in cancerous brain tissues surrounding glioma bulk, respectively. Bar: 50 μm. (For interpretation of the references to colour in this figure legend, the reader is referred to the web version of this article.)

which reached nearly 128% and 146% life-span extension compared with the saline control and Taxol groups, respectively, indicating that dual-targeting PNP–PTX possessed the most powerful anti-tumour activity.

The histopathologic changes in glioma from mice in all treatment groups were examined by the TUNEL assay and H&E staining. As shown in Fig. 11D, for mice treated with PNP–PTX and NP–PTX, significant apoptotic responses of tumour cells and tumour necrosis were clearly observed on day 10. However, little cell apoptosis and negligible necrosis were detected in tumour tissues treated with Taxol compared with the saline control (Fig. 11B&C). Furthermore, much more significant cell apoptosis and tumour necrosis in tumour tissues after day 13 (Fig. 11H) were detected in the PNP–PTX group compared with any other group. In addition, the extent of apoptosis was in accordance with the scope of tumour necrosis.

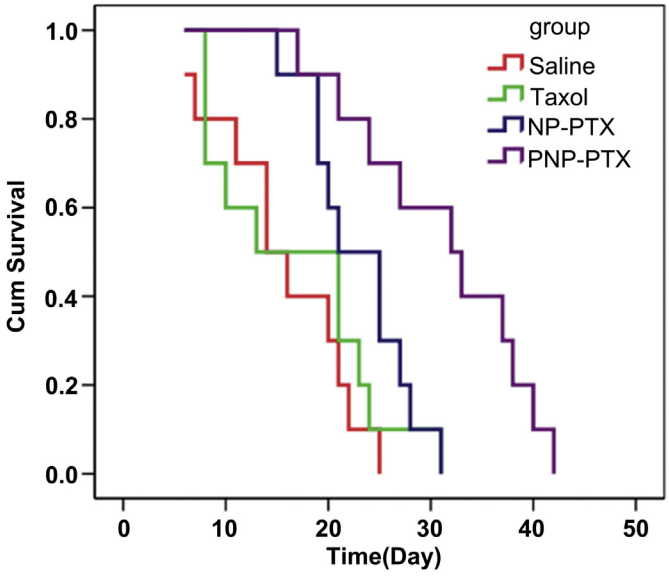

Fig. 10. Survival curve (Kaplan–Meier plot) of the glioma-bearing mice treated with different PTX formulations. (Each was administered 6 mg/kg of PTX at days 5, 8, 11, and 14 post-glioma implantation, $n = 10$).

These results were well in agreement with the life-span extension results, indicating that dual-targeting PNP–PTX could deliver anticancer drugs into glioma cells more efficiently and induced more significant cell apoptosis and tumour necrosis than NP–PTX.

4. Discussion

Non-invasive delivery of therapeutics to the CNS is currently a major challenge, and receptor-mediated transcytosis (RMT) is suitable to shuttle drugs across the BBB to treat brain-associated disorders using the ligands of endogenous receptors at the BBB as potential vectors [48]. Peptide-22 generated by phage display biopanning is a peptide with special affinity for LDLR but without competition with endogenous LDL [30] and might improve CNS targeting and delivery as an LDLR-targeting moiety. However, as a cyclic peptide, it is difficult to be conjugated with nanoparticles without disturbing its spatial structure. Thus, a C6–NH_2 linker was added to the N-terminus of peptide-22, and the covalent attachment of peptide-22 and surface COOH on nanoparticles was accomplished using an EDC/NHS technique [9]. The reduction in zeta potential of NP following its decoration with this negatively charged peptide indicated successful attachment. Further HPLC detection showed that the peptide-22 density on the nanoparticle surface was approximately 248 molecules per nanoparticle, a finding that has proven to be favourable to increase both BBB permeability and intracellular delivery to glioma cells. Considering that other chemical and physical properties of the nanoparticles, including particle size and surface charge, are also important factors that determine the pharmacokinetics (PK) and brain delivery of the nanoparticles, it was of significance to control the nanoparticle size below 150 nm (to approximately 100 nm), which is regarded as most optimal for brain drug delivery [49]. The nanoparticles prepared by blends of Me-PEG–PLA and COOH-PEG–PLA showed an average diameter of approximately 110.8 nm, and there was no significant change in particle size and zeta potential after peptide-22 decoration or coumarin-6 and DiR incorporation. All these results suggested that the dual-targeting system in the present study was suitable for brain delivery.

The success of the dual-targeting delivery system depended on the ability to penetrate the BBB or selectively accumulate at the glioma site by the EPR effect, and then target glioma cells whether

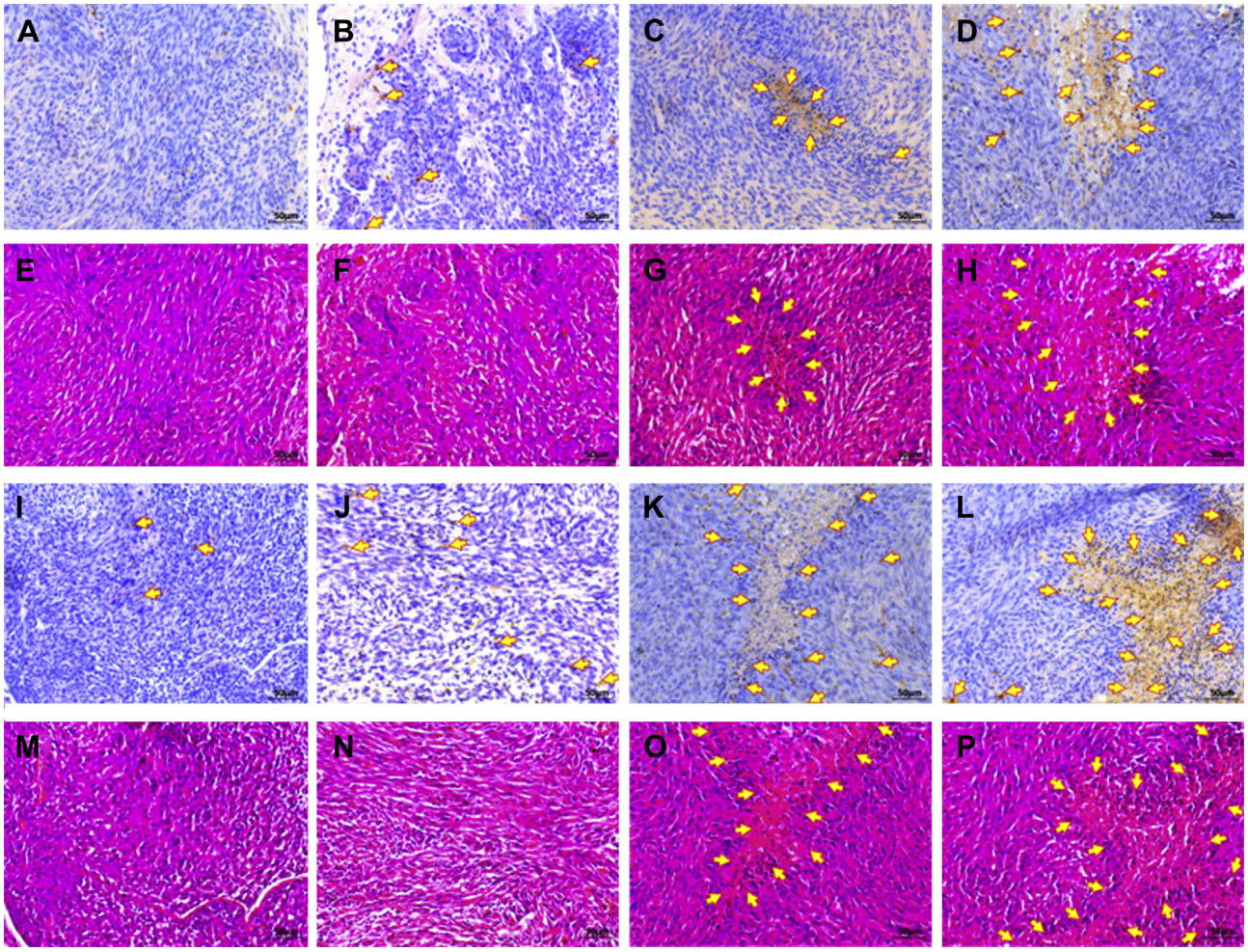

Fig. 11. TUNEL staining and HE staining of glioma tissue sections obtained from mouse models 10 days (upper two rows) and 13 days (lower two rows) post C6 implantation. Each was administered with 6 mg/kg PTX at days 5, 8, 11, and 14 post-C6 cells implantation. Saline control group, (A, E) and (I, M); Taxol treatment, (B, F) and (J, N); NP–PTX treatment, (C, G) and (K, O); PNP–PTX treatment, (D, H) and (L, P). Positive signals were developed by DAB. Cell nuclei were counterstained with haematoxylin. Arrows indicate cell apoptosis body or the scope of necrosis. Bar: 50 μm.

or not the surrounding BBB was disrupted [10,15]. The targeting capability to BBB and glioma cells was evidenced on monolayer cells of BCECs and glioma cells as peptide-22 decoration on the nanoparticle surface could significantly facilitate the uptake of nanoparticles by C6 cells and BCECs. However, the positive results from these experiments might not convincingly represent the BBB permeability and glioma-targeting capability of PNP because the conditions are extremely different from the micro-circumstance found in glioma in vivo. Thus, BCECs were used to construct the BBB model in vitro to evaluate the transport efficiency of different PTX formulations. As a result, after 24 h of incubation, the transport ratio for PNP–PTX was 1.60-fold higher than that for the NP–PTX group and 2.59-fold higher than that for the Taxol group. PNP yielded the most efficient BBB penetration, a finding that might occur through LDLR-mediated transcytosis. The transport rate of PNP mediated by LDLR was similar to Angiopep-2-incorporated nanoparticles mediated by LDLR related protein (LRP) [13], a result that may be partly explained by the two receptors LDLR and LRP belonging to the same family [25] likely functioning in a similar manner. In agreement with the promising results in vitro, the in vivo BBB crossing superiority was demonstrated by much stronger fluorescence signals detected in the brains of those animals administered with DiR-labelled PNP at any time point ranging from 1 h to 10 h post administration compared with the NP group, indicating the potential of PNP to cross the BBB. To better imitate the situation in vivo, a BCECs/C6 glioma co-culture model in vitro was constructed to evaluate the dual-targeting effect of PNP–PTX. The apoptosis induction effect on C6 glioma cells in vitro indicated that PNP–PTX exhibited the strongest dual-targeting effects probably due to improved transcytosis across the BBB and afterwards enhanced endocytosis by glioma cells via active targeting. These results indicated PNP has good potential to cross the BBB, and then target the invasive glioma cells.

To further confirm the dual-targeting effects of PNP in vivo, intracranial C6 glioma tumour-bearing mice were utilised to evaluate the distribution of DiR-labelled nanoparticles. The in vivo imaging of glioma-bearing mice showed PNP could combine the BBB targeting capability and glioma targeting capability and resulted in stronger fluorescence intensity in the brain than NP during 24 h (Fig. 8A). In addition, the ex vivo imaging of the brains harvested at 24 h showed that PNP displayed more intensive fluorescence than NP in the glioma core and in the glioma rim, respectively. The result might be due to PNP penetration into glioma infiltrative region characterised of intact BBB, which could strictly protect the invasive glioma cells from traditional NP. Furthermore, the dual-targeting PNP displayed more precise

glioma targeting and relatively less distribution to normal tissues than NP demonstrated by the glioma/brain fluorescence ratios, which was 3.95 and 2.17 for PNP and NP, respectively. To more intuitively observe the dual-targeting effects of DiR-labelled PNP, the frozen sections of glioma were observed under a fluorescence microscope and a better penetration by DiR-labelled PNP than DiR-labelled NP was detected in both the glioma bulk with a compromised BBB and cancerous tissues surrounding the glioma bulk with an integral BBB (Fig. 9), in consistent with the ex vivo imaging of brains harvested at 24 h after the in vivo imaging (Fig. 8A). All these results suggested that the PNP might achieve efficient and precise brain glioma targeting using two pathways. One pathway involves penetrating the BBB, and then targeting drug delivery to the invasive glioma cells [10], and the other pathway is to exploit the EPR effect in the glioma bulk, eventually reaching glioma cells from the leaky glioma vessels [3,50]. These two pathways maximise glioma cell targeting and minimise the distribution in normal brain tissues, which are extremely useful in glioma imaging and therapy. To further reveal the potential of dual-targeting PNP in glioma therapy, brain tumour-bearing animal models were established and treated with different PTX formulations via systemic administration. Dual-targeting PNP–PTX exhibited the most significant improvement in the median survival time of brain tumour-bearing animals, which reached nearly 128% and 146% life-span extension compared with the saline control and Taxol groups, respectively. By contrast, the Taxol-treated group did not improve the survival significantly compared with the control group. Furthermore, PNP–PTX could induce significantly more cell apoptosis and tumour necrosis as visualised by TUNEL and H&E staining compared with other treatments. In general, these promising results provided robust evidences for efficient therapy for glioma-bearing mice by dual-targeting PNP. The outcomes were in good consistence with in vitro dual-targeting tests and the reasons could be deduced as follows: PNP–PTX is capable of bypassing the BBB without lysosome degradation (Fig. 4) [51] and simultaneously targeting the glioma cell in the site where the BBB is intact or accumulate in the tumour by the EPR effect and then reach the tumour cells via active targeting when the BBB is impaired. NP–PTX is unable to cross the BBB with limited access to the glioma cells invaded into the normal brain tissues and only deposit in the tumour site through the EPR effect when the BBB is compromised.

In this study, the uptake mechanism of PNP by BCECs and C6 cells and the dual-targeting mechanism were both investigated. It was shown that similar cellular uptake mechanisms were involved in PNP uptake into BCECs and C6 cells. PNP uptake by both BCECs and C6 cells was energy-dependant and caveolae- and clathrin-mediated endocytosis but not macropinocytosis were involved in the endocytosis process. The Golgi apparatus and lysosomes have been shown to play important role in both intracellular cargo transport and disposition. In the present study, a Golgi apparatus inhibitor BFA significantly suppressed PNP uptake by C6 cells but have no effect on that by BCECs, indicating the intercellular transport and disposition of PNP in BCECs might be different from that in C6 cells (Fig. 4). A lysosome destroyer monensin did not show inhibitive effect on PNP uptake by both BCECs and C6 cells, which might be useful for PNP to transport across the BBB without degradation and finally to be internalised into glioma cells in vivo. The dual-targeting mechanism was investigated by saturating the LDLR binding site with excess free peptide-22. First, PNP uptake by BCECs and C6 cells could be significantly reduced by pre-incubation with excess free peptide-22. The competitive inhibition effects also occurred in the BBB permeability evaluation and dual-targeting therapy for glioma cells in vitro by the same mechanism. Moreover, the H9c2(2-1) cells with little LDLR expression were chosen as the negative control, and the uptake behaviour of PNP by H9c2(2-1) cells further confirmed PNP uptake was mainly mediated by the interaction between peptide-22 and LDLR over-expressed in BCECs and C6 cells. Considering that peptide-22 was a special ligand for LDLR, the mechanism involved might be receptor-mediated endocytosis [52,53], which may lead to efficient internalisation of ligand-modified nanocarriers in receptor-overexpressing cells [21]. The three types of cells functioned well as experiment models because LDLR expression levels in them consist well with those in mammalian heart, cerebral microvascular endothelial cells and glioma tissues in vivo as reported [16–18,22,25]. Investigating the effect of silencing LDLR expression in LDLR over-expressed cells with siRNA on cellular uptake and penetrating the BBB of PNP may further elaborate the molecular mechanism of LDLR involved PNP's dual targeting to the BBB and glioma cells.

5. Conclusion

We exploited peptide-22 as a targeting moiety to establish a dual-targeting drug delivery system that not only improved the cellular uptake of nanoparticles by C6 cells and BCECs but also enhanced the BBB permeability of PTX and C6 apoptosis below the BBB in vitro. In vivo tests showed dual-targeting PNP exhibited significantly stronger brain permeation, glioma targeting, and enhanced chemotherapeutic effect of PTX compared with those of other groups in glioma mouse models. Altogether, these promising results suggested that the dual-targeting drug delivery system might have great potential for glioma therapy in clinical applications.

Acknowledgements

The work was supported by the National Basic Research Program of China (973 Program, 2013CB932502), National Science and Technology Major Project (2012ZX09304004), National Natural Science Foundation of China (81001404, 81100345) and "Zhuoxue" Program of Fudan University.

References

[1] Wrensch M, Minn Y, Chew T, Bondy M, Berger MS. Epidemiology of primary brain tumors: current concepts and review of the literature. Neuro Oncol 2002;4(4):278–99.
[2] Behin A, Hoang-Xuan K, Carpentier AF, Delattre JY. Primary brain tumours in adults. Lancet 2003;361(9354):323–31.
[3] Agarwal S, Sane R, Oberoi R, Ohlfest JR, Elmquist WF. Delivery of molecularly targeted therapy to malignant glioma, a disease of the whole brain. Expert Rev Mol Med 2013;13:e17.
[4] Agarwal S, Manchanda P, Vogelbaum MA, Ohlfest JR, Elmquist WF. Function of the blood-brain barrier and restriction of drug delivery to invasive glioma cells: findings in an orthotopic rat xenograft model of glioma. Drug Metab Dispos 2013;41(1):33–9.
[5] Donahue MJ, Blakeley JO, Zhou J, Pomper MG, Laterra J, van Zijl PC. Evaluation of human brain tumor heterogeneity using multiple T1-based MRI signal weighting approaches. Magn Reson Med 2008;59(2):336–44.
[6] Yan H, Wang J, Yi P, Lei H, Zhan C, Xie C, et al. Imaging brain tumor by dendrimer-based optical/paramagnetic nanoprobe across the blood-brain barrier. Chem Commun (Camb) 2011;47(28):8130–2.
[7] Groothuis DR. The blood-brain and blood-tumor barriers: a review of strategies for increasing drug delivery. Neuro Oncol 2000;2(1):45–59.
[8] Minchinton AI, Tannock IF. Drug penetration in solid tumours. Nat Rev Cancer 2006;6(8):583–92.
[9] Guo J, Gao X, Su L, Xia H, Gu G, Pang Z, et al. Aptamer-functionalized PEG-PLGA nanoparticles for enhanced anti-glioma drug delivery. Biomaterials 2011;32(31):8010–20.
[10] Gao H, Qian J, Cao S, Yang Z, Pang Z, Pan S, et al. Precise glioma targeting of and penetration by aptamer and peptide dual-functioned nanoparticles. Biomaterials 2013;33(20):5115–23.
[11] Gao H, Qian J, Yang Z, Pang Z, Xi Z, Cao S, et al. Whole-cell SELEX aptamer-functionalised poly(ethyleneglycol)-poly(epsilon-caprolactone) nanoparticles for enhanced targeted glioblastoma therapy. Biomaterials 2012;33(26):6264–72.

[12] Caruso G, Caffo M, Alafaci C, Raudino G, Cafarella D, Lucerna S, et al. Could nanoparticle systems have a role in the treatment of cerebral gliomas? Nanomedicine 2013;7(6):744–52.
[13] Xin H, Jiang X, Gu J, Sha X, Chen L, Law K, et al. Angiopep-conjugated poly(-ethylene glycol)-co-poly(epsilon-caprolactone) nanoparticles as dual-targeting drug delivery system for brain glioma. Biomaterials 2011;32(18): 4293–305.
[14] Ren J, Shen S, Wang D, Xi Z, Guo L, Pang Z, et al. The targeted delivery of anticancer drugs to brain glioma by PEGylated oxidized multi-walled carbon nanotubes modified with angiopep-2. Biomaterials 2012;33(11):3324–33.
[15] Ying X, Wen H, Lu WL, Du J, Guo J, Tian W, et al. Dual-targeting daunorubicin liposomes improve the therapeutic efficacy of brain glioma in animals. J Control Release 2009;141(2):183–92.
[16] Dehouck B, Dehouck MP, Fruchart JC, Cecchelli R. Upregulation of the low density lipoprotein receptor at the blood-brain barrier: intercommunications between brain capillary endothelial cells and astrocytes. J Cell Biol 1994;126(2):465–73.
[17] Gabathuler R. Approaches to transport therapeutic drugs across the blood-brain barrier to treat brain diseases. Neurobiol Dis 2009;37(1):48–57.
[18] Pardridge WM. Molecular biology of the blood-brain barrier. Mol Biotechnol 2005;30(1):57–70.
[19] Sarkar G, Curran GL, Mahlum E, Decklever T, Wengenack TM, Blahnik A, et al. A carrier for non-covalent delivery of functional beta-galactosidase and antibodies against amyloid plaques and IgM to the brain. PLoS One 2013;6(12): e28881.
[20] Spencer BJ, Verma IM. Targeted delivery of proteins across the blood-brain barrier. Proc Natl Acad Sci U S A 2007;104(18):7594–9.
[21] Versluis AJ, Rensen PC, Rump ET, Van Berkel TJ, Bijsterbosch MK. Low-density lipoprotein receptor-mediated delivery of a lipophilic daunorubicin derivative to B16 tumours in mice using apolipoprotein E-enriched liposomes. Br J Cancer 1998;78(12):1607–14.
[22] Maletinska L, Blakely EA, Bjornstad KA, Deen DF, Knoff LJ, Forte TM. Human glioblastoma cell lines: levels of low-density lipoprotein receptor and low-density lipoprotein receptor-related protein. Cancer Res 2000;60(8):2300–3.
[23] Firestone RA. Low-density lipoprotein as a vehicle for targeting antitumor compounds to cancer cells. Bioconjug Chem 1994;5(2):105–13.
[24] Pitas RE, Boyles JK, Lee SH, Hui D, Weisgraber KH. Lipoproteins and their receptors in the central nervous system. Characterization of the lipoproteins in cerebrospinal fluid and identification of apolipoprotein B, E(LDL) receptors in the brain. J Biol Chem 1987;262(29):14352–60.
[25] Hussain MM, Strickland DK, Bakillah A. The mammalian low-density lipoprotein receptor family. Annu Rev Nutr 1999;19:141–72.
[26] Li H, Gray BD, Corbin I, Lebherz C, Choi H, Lund-Katz S, et al. MR and fluorescent imaging of low-density lipoprotein receptors. Acad Radiol 2004;11(11):1251–9.
[27] Corbin IR, Li H, Chen J, Lund-Katz S, Zhou R, Glickson JD, et al. Low-density lipoprotein nanoparticles as magnetic resonance imaging contrast agents. Neoplasia 2006;8(6):488–98.
[28] Crich SG, Lanzardo S, Alberti D, Belfiore S, Ciampa A, Giovenzana GB, et al. Magnetic resonance imaging detection of tumor cells by targeting low-density lipoprotein receptors with Gd-loaded low-density lipoprotein particles. Neoplasia 2007;9(12):1046–56.
[29] Aina OH, Sroka TC, Chen ML, Lam KS. Therapeutic cancer targeting peptides. Biopolymers 2002;66(3):184–99.
[30] Malcor JD, Payrot N, David M, Faucon A, Abouzid K, Jacquot G, et al. Chemical optimization of new ligands of the low-density lipoprotein receptor as potential vectors for central nervous system targeting. J Med Chem 2012;55(5):2227–41.
[31] Okarvi SM. Peptide-based radiopharmaceuticals: future tools for diagnostic imaging of cancers and other diseases. Med Res Rev 2004;24(3):357–97.
[32] Datta G, Chaddha M, Garber DW, Chung BH, Tytler EM, Dashti N, et al. The receptor binding domain of apolipoprotein E, linked to a model class A amphipathic helix, enhances internalization and degradation of LDL by fibroblasts. Biochemistry 2000;39(1):213–20.
[33] Hajek R, Vorlicek J, Slavik M. Paclitaxel (Taxol): a review of its antitumor activity in clinical studies minireview. Neoplasma 1996;43(3):141–54.
[34] Rowinsky EK. Clinical pharmacology of Taxol. J Natl Cancer Inst Monogr 1993;15:25–37.
[35] Nikanjam M, Gibbs AR, Hunt CA, Budinger TF, Forte TM. Synthetic nano-LDL with paclitaxel oleate as a targeted drug delivery vehicle for glioblastoma multiforme. J Control Release 2007;124(3):163–71.
[36] Singla AK, Garg A, Aggarwal D. Paclitaxel and its formulations. Int J Pharm 2002;235(1–2):179–92.
[37] Postma TJ, Heimans JJ, Luykx SA, van Groeningen CJ, Beenen LF, Hoekstra OS, et al. A phase II study of paclitaxel in chemonaive patients with recurrent high-grade glioma. Ann Oncol 2000;11(4):409–13.
[38] Chang SM, Kuhn JG, Robins HI, Schold Jr SC, Spence AM, Berger MS, et al. A phase II study of paclitaxel in patients with recurrent malignant glioma using different doses depending upon the concomitant use of anticonvulsants: a North American brain tumor consortium report. Cancer 2001;91(2): 417–22.
[39] Lu W, Zhang Y, Tan YZ, Hu KL, Jiang XG, Fu SK. Cationic albumin-conjugated pegylated nanoparticles as novel drug carrier for brain delivery. J Control Release 2005;107(3):428–48.
[40] Shi W, Mei H, Deng J, Chen C, Wang H, Guo T, et al. A tissue factor targeted nanomedical system for thrombi-specific drug delivery. Biomaterials 2012;33(30):7643–54.
[41] Mei H, Shi W, Pang Z, Wang H, Lu W, Jiang X, et al. EGFP-EGF1 protein-conjugated PEG-PLA nanoparticles for tissue factor targeted drug delivery. Biomaterials 2010;31(21):5619–26.
[42] Dong Y, Feng SS. Methoxy poly(ethylene glycol)-poly(lactide) (MPEG-PLA) nanoparticles for controlled delivery of anticancer drugs. Biomaterials 2004;25(14):2843–9.
[43] Olivier JC, Huertas R, Lee HJ, Calon F, Pardridge WM. Synthesis of pegylated immunonanoparticles. Pharm Res 2002;19(8):1137–43.
[44] Jiang X, Sha X, Xin H, Chen L, Gao X, Wang X, et al. Self-aggregated pegylated poly (trimethylene carbonate) nanoparticles decorated with c(RGDyK) peptide for targeted paclitaxel delivery to integrin-rich tumors. Biomaterials 2011;32(35):9457–69.
[45] Pang Z, Gao H, Yu Y, Chen J, Guo L, Ren J, et al. Brain delivery and cellular internalization mechanisms for transferrin conjugated biodegradable polymersomes. Int J Pharm 2013;415(1–2):284–92.
[46] Ke W, Shao K, Huang R, Han L, Liu Y, Li J, et al. Gene delivery targeted to the brain using an angiopep-conjugated polyethyleneglycol-modified polyamidoamine dendrimer. Biomaterials 2009;30(36):6976–85.
[47] Xia H, Gao X, Gu G, Liu Z, Hu Q, Tu Y, et al. Penetratin-functionalized PEG-PLA nanoparticles for brain drug delivery. Int J Pharm 2012;436(1–2):840–50.
[48] Gynther M, Ropponen J, Laine K, Leppanen J, Haapakoski P, Peura L, et al. Glucose promoiety enables glucose transporter mediated brain uptake of ketoprofen and indomethacin prodrugs in rats. J Med Chem 2009;52(10): 3348–53.
[49] Hu K, Li J, Shen Y, Lu W, Gao X, Zhang Q, et al. Lactoferrin-conjugated PEG-PLA nanoparticles with improved brain delivery: in vitro and in vivo evaluations. J Control Release 2009;134(1):55–61.
[50] Jain RK, di Tomaso E, Duda DG, Loeffler JS, Sorensen AG, Batchelor TT. Angiogenesis in brain tumours. Nat Rev Neurosci 2007;8(8):610–22.
[51] Dehouck B, Fenart L, Dehouck MP, Pierce A, Torpier G, Cecchelli R. A new function for the LDL receptor: transcytosis of LDL across the blood-brain barrier. J Cell Biol 1997;138(4):877–89.
[52] Moyle WR, Lin W, Myers RV, Cao D, Kerrigan JE, Bernard MP. Models of glycoprotein hormone receptor interaction. Endocrine 2005;26(3):189–205.
[53] Walther TC, Brickner JH, Aguilar PS, Bernales S, Pantoja C, Walter P. Eisosomes mark static sites of endocytosis. Nature 2006;439(7079):998–1003.